Creation of Graphene Plasmons Vortex via Cross Shape Nanoantennas Under Linearly Polarized Incidence

Bofeng Zhu [1,2] · Guobin Ren [1,2] · Yixiao Gao [1,2] · Beilei Wu [1,2] · Yudong Lian [1,2] · Shuisheng Jian [1,2]

Abstract In this paper, we propose a method of creating plasmons vortex on graphene through cross shape nanoantennas under linearly polarized incidence. For each cross shape antenna, the linearly polarized incidence can be coupled to a near-field plasmons vortex on graphene through antenna resonances. When multiple antennas are arranged into a closed circular array, the sign of topological charge of plasmons vortex can be controlled by the linearly polarized direction of incident light with the distribution of absolute field component exhibiting a non-ideal donut profile. The creating of plasmons vortex on graphene may provide new possibilities in various applications, such as the nanoparticles trapping.

Keywords Graphene · Plasmons vortex · Nanoantennas

Introduction

Surface plasmons (SPs) are the surface electromagnetic excitations at metal/dielectric interfaces [1], providing possibilities to achieve strong field confinement and to manipulate the field on a sub-wavelength scale. Graphene, in which a two-

dimensional form of carbon atoms are arranged in a honeycomb lattice [2], has emerged as an alternative material in infrared devices [3]. Compared to the SPs supported on metal surface, graphene plasmons (GPs) have shown many superior properties, such as the strong field confinement [4].

In recent years, the studies on the near-field optical waves carrying orbital angular momentum (OAM), or simply referred to as the plasmons vortex, have made much progress on several aspects, such as the interactions between near-field plasmons and far-field optical vortex [5–7], the circular polarization analyzer [8–10], and the manipulation of dielectric and metal nanoparticles [11, 12]. Within all these works, the plasmons vortex is created via either a geometric phase effect, which is commonly realized by placing plasmons sources into a special format [13–15], or the spin angular momentum carried by the incident circularly polarized light. Recently, Chen et al. have created plasmons vortex through metasurfaces of cross shape apertures under linearly polarized light [16]. Under such circumstance, each antenna itself can be regarded as a plasmons vortex source and together they contribute a vortex at center of antenna arrays, providing another freedom in the creation of plasmons vortex.

One of the most remarkable properties of plasmons vortex is that it could enable the trapping or rotation of nanoparticles [11, 12]; however, due to the weak field confinement and the small electric field gradient of conventional SPs, the trapping force is quite small [17]. In contrast, the tight field confinement and small localized wavelength of GPs could enable the plasmons vortex on graphene to achieve a stronger trapping force as well as a smaller trapping region than the SPs vortex. Therefore, it is meaningful to create the GPs vortex. On the other hand, except for various approaches on exciting plasmons on metal [18–20], GPs can be excited by coupling from incident light via a single nanoantenna [21]. Since the metal antennas are analogies to the apertures in metal surface, by

✉ Guobin Ren
gbren@bjtu.edu.cn

[1] Key Lab of All Optical Network & Advanced Telecommunication Network of EMC, Beijing Jiaotong University, Beijing 100044, China

[2] Institute of Lightwave Technology, Beijing Jiaotong University, Beijing 100044, China

combining all these two studies, the GPs vortex can be obtained under linearly polarized light.

In this paper, we investigate the creation of GPs vortex via cross shape antennas under linearly polarized light. We firstly design in the next section a plasmons vortex source by illuminating a cross shape antenna beneath graphene using linear polarization. Both the phases and amplitudes of plasmons field coupled from the resonances on two arms of antenna are investigated to ensure a desired phase delay between them. The amplitude and phase profiles of single plasmons vortex are further presented. Both the phase and amplitude profiles are compared with the ones excited by two orthogonally placed electric dipoles. In the last section, when multiple antennas are arranged into a closed circular shape formation, a plasmons vortex with opposite topological charge can be created via orthogonal linearly polarized light. In the end, we draw a conclusion.

Single Antenna Under Linear Polarization

Illustrated in Fig. 1 is the schematic view of the cross shape metal antenna. The metal antenna is embedded in a dielectric layer and placed 10 nm below the graphene. In this paper, we assume graphene is placed on $z = 0$ plane. The materials of the metal antenna and dielectric layer are assumed as Au and CaF_2 where the material refractive data is derived from previous measurements [22, 23]. The graphene layer is characterized by a two-dimension surface conductivity ($\sigma_g = \sigma_{intra} + \sigma_{inter}$) material model, in which the graphene thickness is neglected and the σ_{intra} and σ_{inter} are intraband and interband contributions [24]. The graphene Fermi level and carrier relaxation time are respectively set as $E_f = 0.44$ eV and $\tau = 0.5$ ps, which have been used in the previous experimental and theoretical studies [21, 25]. The environmental temperature is $T = 300$ K. The length of two arms of the cross shape antenna along x and y directions are l_x and l_y with the width of arm set as $w = 40$ nm. The incident direction of linearly polarized light is along the z^+ axis. All the numerical calculations

Fig. 1 Schematic view (**a**) and geometrical parameters (**b**) of the cross shape metal antenna

have been performed by the commercial software Lumerical based on FDTD methods and the surrounding boundaries are set as Perfect Matched Layer.

Since the linearly polarized light does not carry any angular momentum component, to create plasmons vortex on graphene by illuminating a cross shape antenna with linear polarization, the resonances of the long and short arms of antenna should have a $\pi/2$ phase delay, which can be introduced by assigning the two arms with different lengths. After the numerical optimization, the length of the two arms are chosen as $l_x = 100$ nm and $l_y = 300$ nm, which are obtained by monitoring the phases of electric field component E_z of GPs above the terminal points of two arms (see the red and black points in the inset of Fig. 2a). To provide a detailed result of such procedure, the dependences of normalized absolute value of phase delay and the amplitude of plasmons electric field component E_z on the incident wavelength are plotted in Fig. 2a, b. The phase delay is normalized to π and the linearly polarized direction of incident light is illustrated with a black arrow. For better presentation, we have also shown in Fig. 2a the results of two non-optimal cases, in which the length l_x is still 100 nm while the lengths l_y are set as 210 and 250 nm, respectively. The incident wavelength spans from $\lambda = 9$ μm to $\lambda = 14$ μm.

As shown in Fig. 2a, the phase delay depends on the incident wavelength and shifts with the length l_y. The zero phase delay exists in the two curves of $l_y = 250$ nm and $l_y = 300$ nm due to the higher order resonances on the long arm of the antenna. Beyond this point, the phase delay firstly increases with the incident wavelength, reaching a plateau and then decreases slightly. There is a phase delay of $\pi/2$ between the plasmons excited by two orthogonal arms of an antenna of $l_y = 300$ nm between wavelength $\lambda = 13$ μm and $\lambda = 14$ μm. For the amplitude of plasmons excited at the shorter arm (the Black Marker), the amplitude decreases continually as the incident wavelength increases. However, for the plasmons excited at the longer arm (the Red Marker), it first decreases rapidly, diving below the amplitude of the short arm and then increases slowly to a plateau, which can be attributed to the conversion between the resonance modes with different orders. It is worth noting that, at the long wavelength region, although the phase delay stays nearly unchanged, the difference between the two amplitudes keeps increasing.

To provide a total field profile of plasmons vortex source under linearly polarized light, we plot the normalized amplitude and phase distribution of electric field component E_z for single cross shape antenna in Figs. 3a–d. The wavelength is $\lambda = 13.4$ μm with the corresponding plasmons localized wavelength is $\lambda_{GP} = 700$ nm, which can be calculated through the Eq. (1) of reference [26], and the corresponding attenuation coefficient is near 1.24 dB/μm [27]. The linearly polarized direction of incident light is marked with white arrow. As
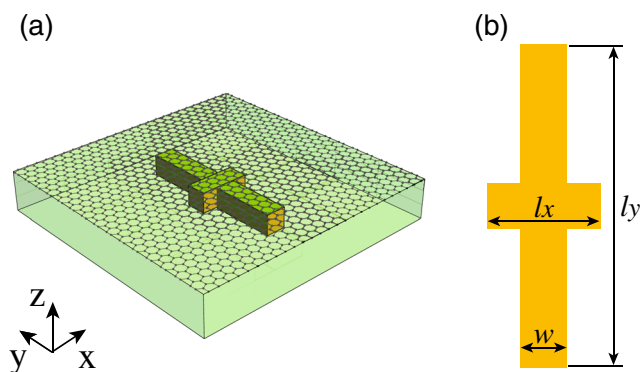
Fig. 2 The dependencies of absolute value of normalized phase delays (**a**) and amplitudes (**b**) of electric field components E_z on the wavelength. In the inset of **a** the positions of monitors and the linearly polarized direction of incidence are illustrated
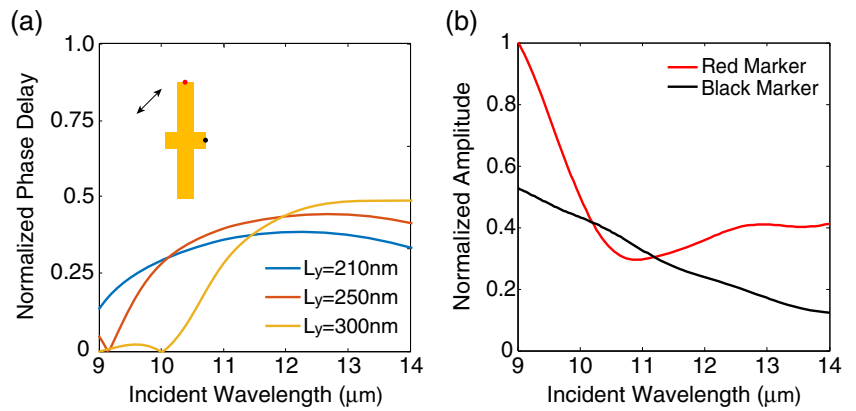

a comparison, in Fig. 3e, f, we also plot the phase profiles of an ideal case, in which two point electrical dipoles with $\pi/2$ phase difference but same amplitude are orthogonally overlapped at the original point above graphene. Corresponding logarithmical distribution of the amplitude of electric field

component $|E_z|$ is shown in the inset of Fig. 3b. In figures, the z coordinates of all the field profiles are $z = 5$ nm.

As shown in Figs. 3a, b, the amplitude of electric field component E_z exhibits sharp change along the rotation direction. The reason originates from the anisotropic resonances of

Fig. 3 The normalized amplitude and phase profiles of electric field component E_z excited by the cross shape antenna under $45°$ (**a**, **c**) and $-45°$ (**b**, **d**) linearly polarized light or the orthogonally placed electrical dipoles (**e**, **f**). The logarithmical distribution of electric field component $|E_z|$ of orthogonally placed electrical dipoles is shown in the inset of **b**. The wavelength is $\lambda = 13.4$ μm
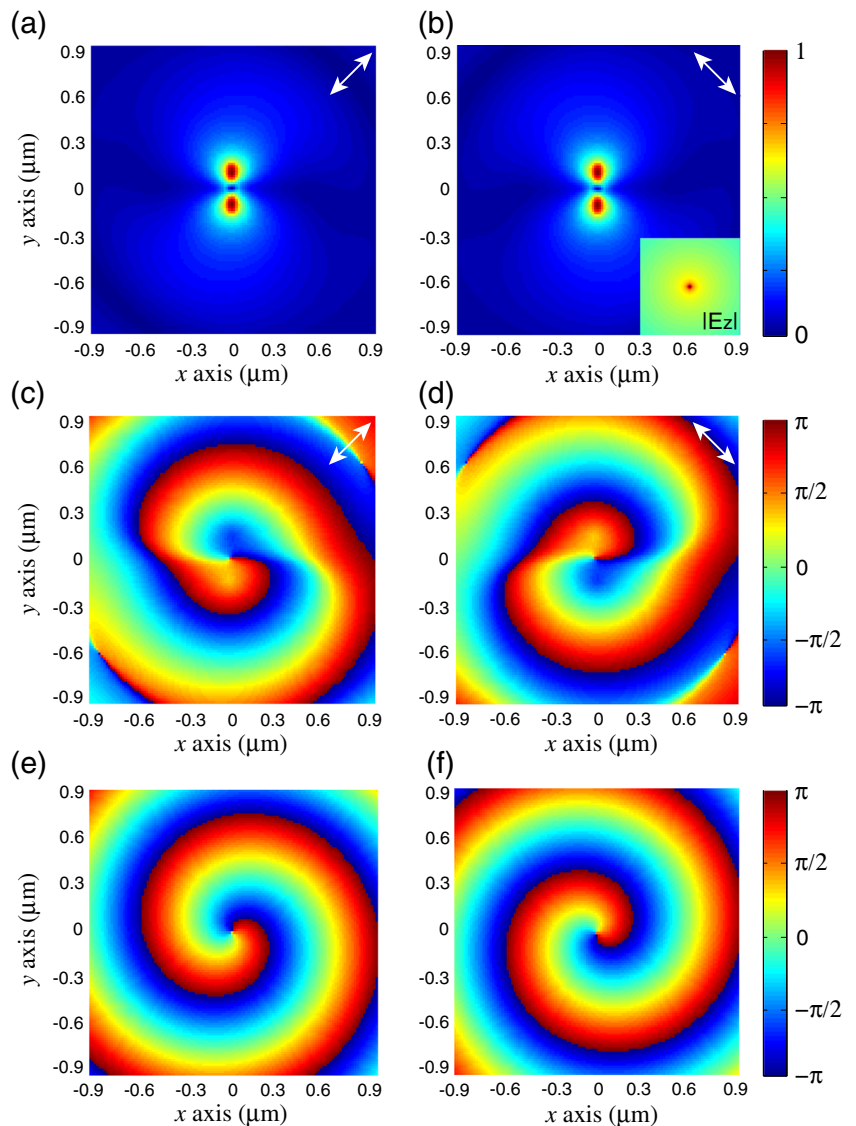
nanoantenna, which is attributed to the difference between the two arm lengths of the antenna. On the other hand, in Fig. 3c or d, we observe that the incident light with orthogonal linearly polarized directions could indeed excite a plasmons vortex on graphene surface through the resonance of cross shape nanoantenna. Such vortex possesses a topological charge of $q = 1$ or $q = -1$, which means there is an azimuthal 2π phase variation around the antenna. However, there is a distortion of phase profile near the center, which also reflects the amplitude difference of excited plasmons along the x and y axis. In contrast, the phase distribution in Fig. 3e or f clearly presents a perfect spiral shape. Meanwhile, based on the results in Fig. 2, we could conclude that the opposite topological charge of plasmons vortex can also be achieved by rotating the cross shape antenna 90° by the z axis and without the need of changing the incident linearly polarized direction.

In our manuscript, the interspace between the nanoantenna and graphene is considerably small for a coupling scheme. Thus, we suppose that further decreasing the interspace may slightly improve the coupling efficiency while only having unobtrusive influences on the field enhancement at the center of nanoantenna arrays. However, reducing the interspace distance also influences the relative phase difference between the plasmons excited by the two arms of cross shape antennas (not shown here). Therefore, for a narrower interspace distance, the geometric structure of the nanoantenna needs to be redesigned to ensure the creation of single plasmons vortex.

One of the superior properties of graphene plasmons to conventional surface plasmons is that their dispersions could be dynamically controlled through electrical biasing. Since in our structure the graphene is placed above the metal antennas, the electrical biasing method can be only implemented by coating the graphene layer with another dielectric layer and polysilicon gating pads on it [28]. With such a scheme, graphene Fermi level can be tuned by bias voltage between polysilicon pads and graphene. By choosing the graphene with lower Fermi level (through lower bias voltage), shorter localized wavelength can be achieved, which is beneficial for improving the coupling efficiency from antennas to graphene plasmons. Meanwhile, the carrier mobility is also a critical factor which determines the attenuation of plasmons graphene. In our modeling of graphene, the carrier mobility of graphene is assumed as $\mu = 10,000$ cm^2/(V·s), which has been adopted in previous investigations on graphene plasmons excitation through dielectric gratings [26]. Lower Fermi level or carrier mobility leads to the larger plasmons attenuation, which may impair the field enhancement effect at center and is not suitable for particles trapping. In the practical applications, the Fermi level should be carefully chosen to achieve a balance between the coupling loss and the plasmons propagation loss.

Circular Cross Shape Antenna Arrays Under Linear Polarization

In the previous section, although a plasmons vortex can be realized on the graphene surface via linearly polarized incidence, the efficiency of coupling incident light to plasmons is quite low due to the limited antenna size. To solve this, one method is to place multiple antennas into a closed circular shape array to produce a nanofocusing effect and enhance the plasmons vortex field at center. Such an antenna array can also be a spiral shape to create a plasmons vortex with zero or higher topological charge [8]. However, for simplicity, in this paper, we only focus on the creation of plasmons vortex with a topological charge of $q = 1$ or $q = -1$ based on a closed circular shape array.

When multiple cross shape antennas are placed into a closed circular shape array, since the optical path from each plasmons source to the center is constant and linearly polarized incidence carries no angular momentum, the azimuthal phase variation at the center of the array only depends on the phase profiles of plasmons field excited by each antenna. Under such circumstance, the plasmons vortex with topological charge of $q = 1$ or $q = -1$ would be created at the center under linearly polarized incidence with orthogonal polarized directions. To verify this, we place an antenna array composed of 17 cross shape antennas with closed circular shape formation beneath the graphene with an interspace distance of 10 nm. All the other implements are the same as those of the case of single antenna in Sec. II. The radius of circular format is set as 1.4 μm and the incident wavelength is $\lambda = 13.4$ μm. The absolute value and phase of field component E_z under different linear polarized directions are presented in Fig. 4. The z coordinates of all the field profiles in figures are $z = 5$ nm. The incidence is 45° (or −45°) linearly polarized, respectively. It should be noted that, for the better present the field distribution at the center of antenna arrays, the fields around the antennas have been saturated.

For the absolute value of field component $|E_z|$, the distribution of which clearly presents a nearly donut shape field with zero values at the center. On the other hand, according to the phase profile of field component E_z at the center in Fig. 4c, d, we conclude that the plasmons vortexes with topological charge of $q = 1$ and $q = -1$ have been created. It is well known that the distribution of field component E_z of a plasmons vortex at the center can be expressed by the qth order Bessel function with the spiral phase profile of $q\varphi$ [14],

$$E_{z,q}(r,\varphi) \propto J_q(k_{GP}r)exp\left[jq\left(\varphi + \frac{\pi}{2}\right)\right], \tag{1}$$

where $k_{GP} = 2\pi/\lambda_{GP}$ is the propagation constant of GPs and (r,φ) is the polar coordinate corresponding to Cartesian coordinate (x, y). According to Eq. (1), when the topological charge of plasmons vortex is $q = 1$ or $q = -1$, the $|E_z|$

Fig. 4 The normalized absolute values (**a**, **c**) and phase profiles (**b**, **d**) of electric field component E_z excited by the closed circular shape antenna arrays under 45 and −45° linear polarizations. The wavelength is $\lambda = 13.4 \ \mu m$
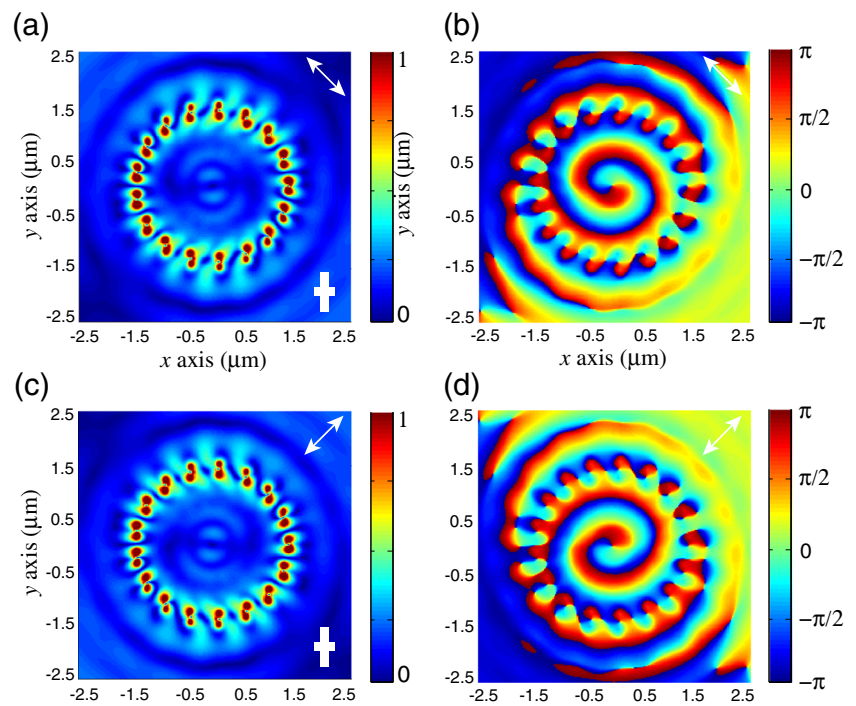
component should be zero at $r = 0$, which is consistent with Fig. 4a, c. On the other hand, it should be noted that the amplitude patterns at the center are not an ideal donut shape. The reason originates from the anisotropic resonant behavior of the antenna, which also results in the hollow field distribution around the antenna in Fig. 3a, b. The quality of noncircular field distribution in Fig. 4 can be improved by increasing the number of antennas in the circular arrays. However, note that at the meantime of increasing antenna numbers, either the geometrical shape of the antenna should be adjusted or the radius of circular should be enlarged. In the former case, one should ensure the $\pi/2$ phase difference between the plasmons excited by two arms. While for the latter case, the plasmons attenuation would increase, which may impair the field enhancement at center and the particles trapping effect.

Conclusions

In conclusion, we report the creation of plasmons vortex on graphene through cross shape antenna under linearly polarized incidence. For singular cross shape antenna under linearly polarized incidence, a plasmons vortex can be excited on graphene by assigning the two arms of antenna with different lengths and therefore achieving a $\pi/2$ phase delay. Although the plasmons vortex created by a single antenna can be clearly observed, a slightly distortion appears due to the difference in amplitudes of plasmons field excited by two arms. By arranging multiple antennas into a closed circular shape format, plasmons vortex with topological charge of $q = 1$ or $q = -1$

can be created at the center and accordingly, the absolute value of plasmons electric field component exhibits a donut shape distribution. The topological charge of graphene plasmons can be controlled by adjusting the linearly polarized direction. The creation of plasmons vortex on graphene may provide possibilities in applications such as particle manipulation.

References

1. Maier SA (2007) Plasmonics: fundamentals and applications. Springer, New York
2. Novoselov KS, Geim AK, Morozov SV, Jiang D, Katsnelson MI, Grigorieva IV, Dubonos SV, Firsov AA (2005) Two-dimensional gas of massless Dirac fermions in graphene. Nature 438(7065): 197–200. doi:10.1038/nature04233
3. Grigorenko AN, Polini M, Novoselov KS (2012) Graphene plasmonics. Nat Photonics 6(11):749–758. doi:10.1038/nphoton.2012.262
4. Vakil A, Engheta N (2011) Transformation optics using graphene. Science 332(6035):1291–1294. doi:10.1126/science.1202691
5. Yu H, Zhang H, Wang Y, Han S, Yang H, Xu X, Wang Z, Petrov V, Wang J (2013) Optical orbital angular momentum conservation during the transfer process from plasmonic vortex lens to light. Sci Rep 3:3191. doi:10.1038/srep03191
6. Cho SW, Park J, Lee SY, Kim H, Lee B (2012) Coupling of spin and angular momentum of light in plasmonic vortex. Opt Express 20(9):10083–10094. doi:10.1364/OE.20.010083
7. Zilio P, Parisi G, Garoli D, Carli M, Romanato F (2014) Bilayer holey plasmonic vortex lenses for the far field transmission of pure

orbital angular momentum light states. Opt Lett 39(16):4899–4902. doi:10.1364/OL.39.004899

8. Chen W, Rui G, Abeysinghe DC, Nelson RL, Zhan Q (2012) Hybrid spiral plasmonic lens: towards an efficient miniature circular polarization analyzer. Opt Express 20(24):26299–26307. doi:10.1364/OE.20.026299

9. Yang S, Chen W, Nelson RL, Zhan Q (2009) Miniature circular polarization analyzer with spiral plasmonic lens. Opt Lett 34(20): 3047–3049. doi:10.1364/OL.34.003047

10. Chen W, Abeysinghe DC, Nelson RL, Zhan Q (2010) Experimental confirmation of miniature spiral plasmonic lens as a circular polarization analyzer. Nano Lett 10(6):2075–2079. doi:10.1021/nl100340w

11. Dienerowitz M, Mazilu M, Reece PJ, Krauss TF, Dholakia K (2008) Optical vortex trap for resonant confinement of metal nanoparticles. Opt Express 16(7):4991. doi:10.1364/oe.16.004991

12. Tsai WY, Huang JS, Huang CB (2014) Selective trapping or rotation of isotropic dielectric microparticles by optical near field in a plasmonic Archimedes spiral. Nano Lett 14(2):547–552. doi:10.1021/nl403608a

13. Chen-Da K, Wei-Lun H, Jer-Shing H, Chen-Bin H (2013) Deterministic synthesis of optical vortices in tailored plasmonic Archimedes spiral. IEEE Photon J 5(3):4800409–4800409. doi:10.1109/jphot.2013.2261802

14. Kim H, Park J, Cho SW, Lee SY, Kang M, Lee B (2010) Synthesis and dynamic switching of surface plasmon vortices with plasmonic vortex lens. Nano Lett 10(2):529–536. doi:10.1021/nl903380j

15. Rui G, Zhan Q, Cui Y (2015) Tailoring optical complex field with spiral blade plasmonic vortex lens. Sci Rep 5:13732. doi:10.1038/srep13732

16. Chen CF, CT K, Tai YH, Wei PK, Lin HN, Huang CB (2015) Creating optical near-field orbital angular momentum in a gold metasurface. Nano Lett 15(4):2746–2750. doi:10.1021/acs.nanolett.5b00601

17. Yang X, Liu Y, Oulton RF, Yin X, Zhang X (2011) Optical forces in hybrid plasmonic waveguides. Nano Lett 11(2):321–328. doi:10.1021/nl103070n

18. Chen WT, PC W, Chen CJ, Chung HY, Chau YF, Kuan CH, Tsai DP (2010) Electromagnetic energy vortex associated with subwavelength plasmonic Taiji marks. Opt Express 18(19):19665–19671. doi:10.1364/OE.18.019665

19. Zayats AV, Smolyaninov II, Maradudin AA (2005) Nano-optics of surface plasmon polaritons. Phys Rep 408(3–4):131–314. doi:10.1016/j.physrep.2004.11.001

20. Hsu WL, PC W, Chen JW, Chen TY, Cheng BH, Chen WT, Huang YW, Liao CY, Sun G, Tsai DP (2015) Vertical split-ring resonator based anomalous beam steering with high extinction ratio. Sci Rep 5:11226. doi:10.1038/srep11226

21. Alonso-Gonzalez P, Nikitin AY, Golmar F, Centeno A, Pesquera A, Velez S, Chen J, Navickaite G, Koppens F, Zurutuza A, Casanova F, Hueso LE, Hillenbrand R (2014) Controlling graphene plasmons with resonant metal antennas and spatial conductivity patterns. Science 344(6190):1369–1373. doi:10.1126/science.1253202

22. Li HH (1980) Refractive index of alkaline earth halides and its wavelength and temperature derivatives. J Phys Chem Ref Data 9(1):161–287. doi:10.1063/1.555616

23. Palik, ED (1985) Handbook of Optical Constants of Solids, vol 1. Academic Press

24. Hanson GW (2008) Dyadic Green's functions and guided surface waves for a surface conductivity model of graphene. J Appl Phys 103(6):064302. doi:10.1063/1.2891452

25. Nikitin AY, Alonso-Gonzalez P, Hillenbrand R (2014) Efficient coupling of light to graphene plasmons by compressing surface polaritons with tapered bulk materials. Nano Lett 14(5):2896–2901. doi:10.1021/nl500943r

26. Gao W, Shu J, Qiu C, Xu Q (2012) Excitation of plasmonic waves in graphene by guided-mode resonances. ACS Nano 6(9):7806–7813. doi:10.1021/nn301888e

27. Ming-Jun L, Xin C, Anping L, Gray S, Ji W, Walton DT, Zenteno LA (2009) Limit of effective area for single-mode operation in step-index large mode area laser fibers. J Lightwave Technol 27(15): 3010–3016. doi:10.1109/jlt.2009.2020682

28. Gomez-Diaz JS, Perruisseau-Carrier J (2013) Graphene-based plasmonic switches at near infrared frequencies. Opt Express 21(13): 15490–15504. doi:10.1364/OE.21.015490